Highly subwavelength, superdirective cylindrical nanoantenna

Samel Arslanagić[1] and Richard W. Ziolkowski[2,3]

[1] *Technical University of Denmark, Lyngby, Denmark*
[2] *University of Technology Sydney, Ultimo NSW 2007, Australia*
[3] *The University of Arizona, Tucson, AZ, 85721 USA*

A superdirective cylindrical nanoantenna is demonstrated with a multilayered cylindrical metamaterial-inspired structure. Targeting specific scattering coefficients for the dipole and higher order modes, the ideal limit of needle radiation is demonstrated. A five-layer system is optimized to demonstrate its approach to the theoretical directivity bound. While the resulting structure is scalable to any frequency regime, its highly subwavelength overall size ($\lambda_0/10$) takes advantage of combinations of positive and negative permittivity materials in the optical regime.

The ability to control passive and active nanosystems has far-reaching importance in several emerging fields of science and engineering, as well as to applications with high societal benefit. Significant interest has thus emerged in developing optical nanoantennas to control light-matter interactions [1]. Highly directive optical elements have been shown to have many impactful applications, for example, enhanced Raman spectroscopy [2], emission enhancement of single photons [3, 4], ultra-sensitive sensing [5, 6], enhanced photo-detection [7], remote sensing [8], and wireless power transmission [9]. Several classic antenna approaches [10] to achieving higher directivity at optical frequencies have been reported. These include Yagi-Uda nanoantennas [11, 12] and nanoantenna arrays [13, 14]. A variety of electric and magnetic dipolar and mutipolar approaches have also been considered [15–23]. The former yield electrically large systems. The latter yield higher maximum directivity values or higher front-to-back ratios (FTBRs), but have multiple large sidelobes or broad radiation patterns. In contrast, we have developed a highly subwavelength, single element with needle–like radiation performance.

This goal was achieved by combining the metamaterial-inspired paradigm [24] that employs near-field resonant parasitic (NFRP) elements to enhance and control the emissions from a driven source with the concept of having those elements generate higher order modes (HOMs) [25]. However, in contrast to the array of elemental Huygens multipole radiators investigated in [25], we consider herein the use of a single multilayered cylindrical highly subwavelength structure as the NFRP element driven by a line source to achieve the desired needle-like performance. Since the objective is to demonstrate its superdirective (i.e., directivity larger than that of a reference antenna system of the same size excited with a uniform amplitude and phase) capabilities, both the source and the structure are assumed infinite to simplify the analysis and design. Through the simultaneous excitation of its dipole and HOMs at the desired frequency in a single, properly designed multilayered structure, superdirective radiation is demonstrated, i.e., the cylindrical waves emitted by the source are transduced into a highly collimated beam.

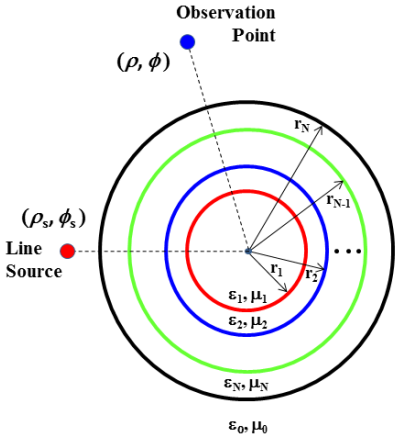

FIG. 1. Line source excited N-layer, $N+1$ region, 2D concentric cylinder structure.

The multi-layer scattered field coefficients are developed based on both Dirac–delta and binomial distributions to illustrate being able to tailor the characteristics of the resulting radiation performance by design in analogy with classic array theory [10]. We demonstrate that those multi-element array behaviors can be emulated with these multi-layered structures. In contrast to previous superdirective studies, e.g., [15, 20, 22], that considered higher directivity from spherical single-layer plasmonic or all-dielectric core-shell structures by exciting individual electric and magnetic dipole or HOMs, it is demonstrated herein that a Dirac–delta based multilayer NFRP nanoantenna can produce not only high directivity, but needle–like radiation patterns with very low sidelobe levels by combining properly weighted combinations of the dipole and several HOMs whose availability is facilitated by the thicknesses and material properties of those multi-layers. Moreover, the cylindrical geometry and its natural polarization selectivity enable applications not accessible with their highly symmetric spherical counterparts. A five-layer, metamaterial-inspired structure is optimized to demonstrate approaching the theoretical directivity bound in practice.

A cross section of the two-dimensional (2D) based

canonical configuration of interest is depicted in Fig. 1. As an $N+1$ region configuration, it is the general case. It consists of a circularly cylindrical core of radius r_1 (Region 1) covered with $N-1$ concentric layers, Region j with outer radius r_j , $j = 2, ..., N$. These N layers are embedded in an infinite ambient host medium (Region $N+1$). A cylindrical coordinate system, (ρ, ϕ, z), is introduced. The axes of the cylinders coincide with the z-axis. Region i, with $i = 1, 2, ..., N$, is characterized by a permittivity and a permeability. Assuming the $\exp(j\omega t)$ time dependence throughout, they are denoted by $\epsilon_i = \epsilon_i' - j\epsilon_i''$ and $\mu_i = \mu_i' - j\mu_i''$, respectively, and a wavenumber $k_i = \omega\sqrt{\epsilon_i}\sqrt{\mu_i}$. The host medium, Region $N+1$, without any loss of generality is taken to be free-space with permittivity ϵ_0 and permeability μ_0. The cylindrical regions are excited by an infinite, z-oriented line source located in Region $N+1$. Thus, the wave number in the source region is the free-space wave number $k_{N+1} = k_0 = \omega\sqrt{\epsilon_0\mu_0}$. In the time harmonic case the source is characterized by the frequency f_0 and the corresponding free-space wavelength $\lambda_0 = c/f_0$, where c is the speed of light in vacuum: $c = 1/\sqrt{\epsilon_0\mu_0}$. Consequently, the free-space wave number is also $k_0 = 2\pi/\lambda_0$.

The excitation is taken to be a magnetic line source (MLS). Consequently, only TE^z polarized fields and dielectric layers are considered. A more general discussion is provided in [26]. The coordinates of the line source are (ρ_s, ϕ_s), while those of the observation points are (ρ, ϕ). The MLS is defined by the constant magnetic current $I_{\rm MLS} = 1.0\,[V]$.

Fields in a cylindrical geometry can be decomposed into cylindrical harmonics. Because of the restriction to two dimensions and the azimuthal symmetry, only three of the six electromagnetic field components (H_z, E_ρ, E_ϕ) are needed to characterize any given TE^z field. In fact, only the H_z component of the field and derivatives of it are needed to characterize the TE^z source and scattered fields. The main steps of the analytical solution of this canonical scattering problem are reviewed in [26] and outlined in general, e.g., in [27]. Since only the total magnetic field in the exterior region is needed for the directivity outcome, the source $(E_\rho^{\rm MLS}, E_\phi^{\rm MLS})$ and scattered $(E_\rho^{\rm scat}, E_\phi^{\rm scat})$ electric field components, which are readily obtained from these magnetic fields, are not included here. They are provided for completeness along with the solution process for determining the unknown expansion coefficients in [26].

The magnetic source and scattered field pieces in the exterior region are explicitly:

$$\boldsymbol{H}_{\rm MLS}(\rho,\phi) = -\hat{z}\, I_{\rm MLS}(\omega)\,\frac{\omega\varepsilon_{N+1}}{4} \tag{1}$$
$$\times \begin{cases} \sum_{m=0}^{\infty} \tau_m\, J_m(k_{N+1}\rho)\, H_m^{(2)}(k_{N+1}\rho_s)\, \cos[m(\phi-\phi_s)] \\ \quad \text{for } \rho \le \rho_s \\ \sum_{m=0}^{\infty} \tau_m\, J_m(k_{N+1}\rho_s)\, H_m^{(2)}(k_{N+1}\rho)\, \cos[m(\phi-\phi_s)] \\ \quad \text{for } \rho \ge \rho_s \end{cases}$$

$$\boldsymbol{H}^{\rm scat}(\rho,\phi) = -\hat{z}\, I_{\rm MLS}(\omega)\,\frac{\omega\varepsilon_{N+1}}{4} \tag{2}$$
$$\times \sum_{m=0}^{\infty} \tau_m\, A_m^{N+1} H_m^{(2)}(k_{N+1}\rho)\, \cos[m(\phi-\phi_s)]$$

where $H_m^{(2)}(\cdot)$ is the Hankel function of second kind, order m, and A_m^{N+1} are the expansion coefficients of the scattered field and where $\tau_0 = 1$ and $\tau_m = 2$ for $m \neq 0$. Once the source and scattered field coefficients are known, a variety of figures of merit can be derived. The exact infinite series solution is truncated to a finite number of modes in practice after justifying that the higher order ones have little impact on those outcomes.

The directivity is the quantity of major interest here. It is defined as the ratio of the radiation intensity in a given direction to the radiation intensity averaged over all directions. With $\boldsymbol{H}_{\rm tot}^{\rm ff} = [\,\boldsymbol{H}_{\rm MLS} + \boldsymbol{H}_{\rm scat}\,]^{\rm ff}$ being the total magnetic far-field in the exterior region [26], the directivity for the MLS-excited N-layered cylinder is

$$D_N(\phi) = \frac{2\pi\,\rho\,\left|\,\boldsymbol{H}_{\rm tot}^{\rm ff}(\rho,\phi)\,\right|^2}{\int_0^{2\pi}\left|\,\boldsymbol{H}_{\rm tot}^{\rm ff}(\rho,\phi)\,\right|^2\,\rho\,d\phi} \tag{3}$$
$$= \frac{\left|\sum_{m=0}^{\infty}\,\tau_m\,j^m\,\left[\,J_m(k_0\rho_s) + A_m^{N+1}\,\right]\,\cos[m(\phi-\phi_s)]\,\right|^2}{\sum_{m=0}^{\infty}\,\tau_m\,\left|J_m(k_0\rho_s) + A_m^{N+1}\right|^2}$$

It is emphasized that the exterior region scattered field coefficients A_m^{N+1} depend on the field coefficients associated with each of the N layers.

Let $\psi = \phi_{\max} - \phi_s$, where $\phi_{\max}$ is the direction into which one would like to have the maximum directivity. Then the parameters of the material layers (their thickness and permittivities) will be tailored to produce scattering coefficients yielding a desired directivity pattern. We begin with the choices that lead to a Dirac-delta outcome in a specified direction. Recall from the theory of distributions [28] that

$$\delta(x-a) = \frac{1}{2\pi}\; + \frac{1}{\pi}\,\sum_{m=1}^{\infty}\cos[\,m\,(x-a)\,] \tag{4}$$

This suggests setting the Dirac-delta based coefficients $A_{m,\delta}^{N+1}$ to:

$$\begin{aligned} A_{0,\delta}^{N+1} &= \frac{1}{2\pi} - J_0(k_0\rho_s) \\ A_{m,\delta}^{N+1} &= \frac{1}{\tau_m\,\pi\,j^m}\cos(m\psi) - J_m(k_0\rho_s) \quad \text{for } m > 0 \end{aligned} \tag{5}$$

The directivity for the N-layer problem with the sum truncated to $N+1$ terms then becomes

$$D_N(\phi) \approx \frac{\left|\,1 + 2\,\sum_{m=1}^{N}\,\cos(m\psi)\,\cos[m(\phi-\phi_s)]\,\right|^2}{1 + 2\,\sum_{m=1}^{N}\,|\,\cos(m\psi)\,|^2} \tag{6}$$

With the desire to have the cylinder system convert the line source field into a directive beam, it is natural and most effective to have the beam direction pointed away from the source. The angles which finalize the scattering coefficients (5) are thus explicitly set to $\phi_s = \pi$ and $\phi_{\max} = 0$ without any loss of generality. Since $\psi = -\pi$, one then has $1 + 2\sum_{m=1}^{N} |\cos(-m\pi)|^2 = 1 + 2N$ and the directivity becomes

$$D_N(\phi) \approx \frac{\left| 1 + 2\sum_{m=1}^{N} \cos(m\phi) \right|^2}{1 + 2N} \tag{7}$$

One recognizes immediately from (4) that as $N \to \infty$ in (7), needle radiation in the $\phi = 0$ direction is obtained, i.e., $D_{N\to\infty}(\phi) \propto \delta(\phi)$. The maximum directivity for a finite number of layers N is

$$D_{N,\max}(\phi = 0) \approx \frac{\left| 1 + 2\sum_{m=1}^{N} 1 \right|^2}{1 + 2N} = 2N + 1 \tag{8}$$

which, as derived in [26], is the theoretical maximum for two dimensions. A comparison of the directivities (in dB units) as functions of the observation angle ϕ exhibited by the $N = 5, 10, 100,$ and 1000, layer cases is shown in Fig. 2. The maximum directivity in each case is confirmed to be 11, 21, 201 and 2001, i.e., $2N + 1$. The FTBR, i.e., $D_N(\phi = 0°)/D_N(\phi = 180°)$, for each case is, respectively, 20.83, 26.44, 46.06 and 66.02 dB. The $N = 1000$ case clearly demonstrates its needle-like behavior.

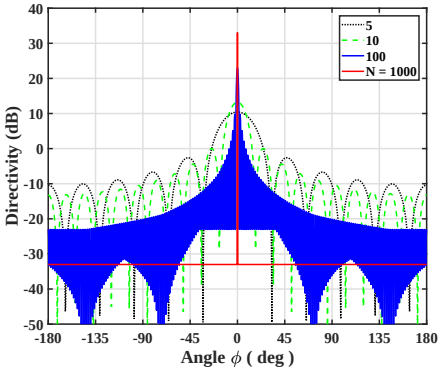

FIG. 2. Comparison of the directivity generated by the Dirac-delta coefficients associated with the $N = 5$, $N = 10$, $N = 100$, and $N = 1000$ layer structures.

It is well-known that the amplitude and/or phase distributions between the elements of an antenna array can be designed to control its radiation characteristics [10]. Common amplitude distributions for broadside radiating, uniformly spaced arrays are the uniform (largest directivity), Dolph-Tschebyscheff (specified flat side-lobe level), and binomial (few or no sidelobes). To demonstrate that the scattering coefficients of the multi-layer structure can be weighted to produce other beams tailored by choice, a binomial distribution was also considered. The weights of a binomial configuration with N modes are:

$$p_m^N = \frac{(N-1)!}{m!(N-1-m)!}, \qquad m = 0, 1, ..., N-1 \tag{9}$$

which correspond to the expansion coefficients of the polynomial $(1 + x)^{N-1}$ [10, 6-62]. Proceeding as we did with the Dirac-delta based coefficients, the radiation intensity of the line source-multilayered cylinder system will have a binomial-distribution behavior if the scattered field coefficients are:

$$A_{m,\text{binom}}^{N+1} = j^{-n} \frac{p_m^N}{\max p_m^N} \cos m\psi - J_m(k_0\rho_s) \tag{10}$$

where each term has been normalized by the largest one: $\max\{p_m^N/\tau_m\}$.

The directivities associated with the Dirac-delta and binomial-distribution based scattered field coefficients for $N = 10$ layers are compared in Fig. 3(a). The Dirac-delta coefficients produce a more directive, more tightly confined main beam (first null appears at $\phi_{\text{null}} = 2\pi/(2N+1)$) with lower sidelobes. On the other hand, the binomial case is broader but has fewer sidelobes. The corresponding maximum directivity as the number of layers N (hence, modes) increases, which was obtained by calculating the directivity (3) with those coefficients and finding the maximum value, is shown in Fig. 3(b). The $D_{N,\max}$ values achieve their upper bounds $2N + 1$ in each Dirac-delta case. The directivity of the binomial coefficient-based beam clearly begins to saturate as the number of layers (hence, modes) increases. In contrast to the equal power weighting associated with each Dirac-delta mode, the binomial weights decrease as the mode number increases. These coefficient choices clearly demonstrate the ability to customize the output beam of the system simply by tailoring the scattering coefficients through the geometry and material choices in analogy with amplitude tapering in a classic antenna array. Several multilayered cylinder configurations were explored to illustrate their potential to achieve these highly directive behaviors. Considering the degrees of freedom in the system, the number of modes that one can generate on demand and control is directly tied to the number of layers of the structure and the materials from which it is made. In principle, N layers can be optimized to generate at least $N + 1$ modes of significance with the desired amplitudes and phases. As demonstrated in [26], the remaining modes contribute little to the overall scattering since they are not designed to resonate with the source in any way. The mode sums are then truncated and limited to the $m = 0, 1, \ldots, N$ terms.

A highly subwavelength, MLS-excited, $N = 5$ layer, lossless structure, whose exterior radius was fixed to be $r_5 = \lambda_0/10$, was investigated. This electrically small system has a transverse effective width $W_{\text{eff}} = 2\,r_5 = \lambda_0/5$.

The MLS is located at $(\rho, \phi) = (1.05\, r_5, 180°)$, far enough away from the origin to produce several HOMs. As derived in [26], the directivity of the analogous uniformly excited two-dimensional antenna system is $D_{2D} = 2\pi W_{\text{eff}}/\lambda_0$. Consequently, any 5-layered configuration that yields a directivity greater than $D_{2D} = 1.257$ is superdirective [10]. If it approaches the maximum: $D_{N=5,\max} = 11 = 8.75\, D_{2D}$, it is needle-like. Since the structure and results are defined in terms of λ_0, they scale to any frequency. In particular, for an optical source with $\lambda_0 = 500\ nm$, the cylindrical nanoantenna has a 50 nm radius.

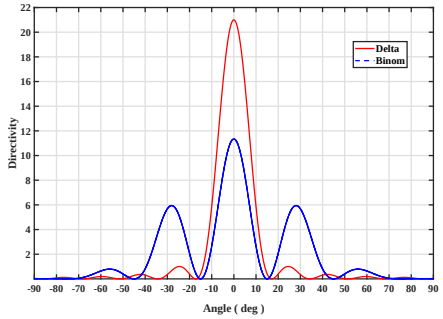

(a)

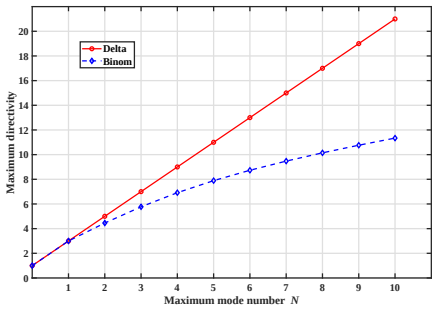

(b)

FIG. 3. Directivity obtained for the Dirac-delta and binomial-distribution based scattered field coefficients. (a) Patterns for $N = 10$. (b) Maximum directivity as the maximum mode number N varies. (Linear scales)

The optimization process is detailed in [26]. The material choices take advantage of the known miniaturization capabilities associated with the juxtaposition of positive and negative material regions [29] which naturally are available in the optical regime. The relative permittivities in the five-layer structure were determined to be: $\varepsilon_{1r} = 6.618, \varepsilon_{2r} = -6.651, \varepsilon_{r3} = -4.622, \varepsilon_{r4} = 39.864, \varepsilon_{r5} = -49.979$, when the radii of the layers were specified to be: $r_1 = 0.015\lambda_0, r_2 = 0.030\lambda_0, r_3 = 0.070\lambda_0, r_1 = 0.085\lambda_0, r_5 = 0.10\lambda_0$. The corresponding $m = 0, 1, \ldots, 5$ scattering coefficients were obtained and used to calculate (6). A comparison of the directivity determined with these numerically obtained scattering coefficients and the Dirac-delta based ones (5) for this MLS-excited 5-layer cylindrical scattering structure is given in Fig. 4. The maximum $D_{\text{N=5,max}} = 10.686 = 8.5\, D_{2D}$ occurs along the $\phi = 0°$ direction and the associated FTBR $= 54.83 = 17.39\ dB$. These results demonstrate that this multilayered cylinder acts as a superdirective lens element that transduces the cylindrical waves from the MLS into a highly directive beam.

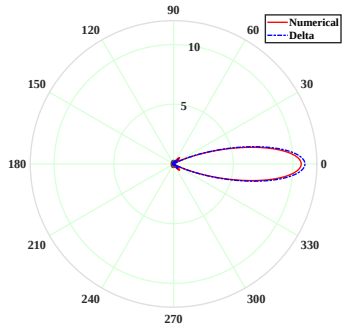

FIG. 4. Comparisons of the directivity obtained with only the $m = 0, 1, \ldots, 5$ numerically obtained and the Dirac-delta based scattering coefficients for the MLS-excited, 5-layer highly subwavelength cylinder. (Linear scale)

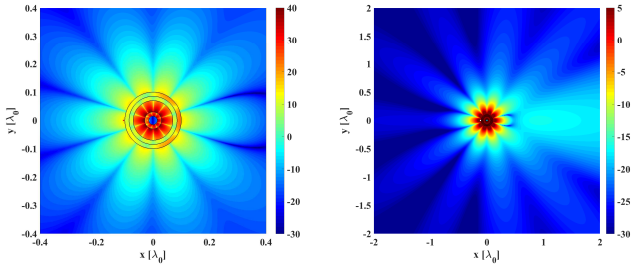

(a) (b)

FIG. 5. Plots of $10 \log_{10} |H_z(x, y)|$ for the MLS-excited, 5-layer highly subwavelength cylinder. (a) Near field (red dot denotes the source location). (b) Far field (white dot denotes the source location).

The near and mid field distributions of the magnitude of the total magnetic field: $10 \log_{10} |H_z^{\text{tot}}(x, y)|$ (i.e., in dB units), of the optimized 5-layer structure are shown in Figs. 5(a) and 5(b), respectively. From the near field plot, one immediately recognizes that the $N = 5$ mode is quite dominant in the vicinity of the structure and the total field is strongly excited around the $\phi = 0$ direction in layer 5. Furthermore, one begins to see in the mid-range results that the main beam is becoming dominant and the sidelobes are beginning to disappear. Thus, while the $N = 5$ mode is necessary for the large $D_{\max}$ value, the lower order modes are necessary with the correct weighting to significantly reduce the sidelobe levels. Furthermore, the superdirective behavior is obtained with only one set of field modes; the complementary TM^z set is not present. These results reaffirm similar conclusions given in [25].

It is again noted that only the modes $N = 0, 1, \cdots, 5$

were superimposed to obtain all of these results. More HOMs would be required only if more layers were included in the configuration. It is further illustrated in [26] that as the overall size of the structure is allowed to be larger, one can demonstrate not only this highly directive behavior with only positive material layers, but even super-backscattering [30].

Large epsilon-negative (ENG) and positive permittivity values are naturally available at optical frequencies from both metals and resonant polaritonic materials. However, these optical materials are generally very lossy. While they do not impact the ratio of the radiated powers, large losses have detrimental effects on a structure's ability to promote the presence of the HOMs. Hence, losses negatively impact the overall directivity. Nevertheless, by introducing gain into an optical structure, these deleterious loss effects can be mitigated. Consequently, a practical demonstration of these superdirective outcomes should be focused on those frequencies. The resulting highly directive optical nanoantennas would have many potential photonics applications ranging from sensors and microscopy to integrated optical circuits. On the other hand, many natural and artificially-realized very small and large positive and negative permittivity, low loss materials are now available at microwave and millimeter wave frequencies. The ability to achieve superdirective beams from electrically small systems would have many practical applications in current and future wireless systems. Thus, the reported developments are also very relevant to those lower frequency bands.

[1] M. Agio and A. Alù, *Optical Antennas* (Cambridge University Press: Cambridge, UK, 2013).
[2] A. Ahmed and R. Gordon, Nano Lett. **12**, 2625 (2012).
[3] Y. C. Jun, K. C. Huang, and M. L. Brongersma, Nat. Commun. **2**, 283 (2011).
[4] A. G. Curto, T. H. Taminiau, G. Volpe, M. P. Kreuzer, R. Quidant, and N. F. Van Hulst, Nat. Commun. **4**, 1750 (2013).
[5] P. Zijlstra, P. M. Paulo, and M. Orrit, Nat. Nanotechnol. **7**, 379 (2012).
[6] C. Wu, A. B. Khanikaev, R. Adato, N. Arju, A. A. Yanik, H. Altug, and G. Shvets, Nat. Mater. **11**, 69 (2012).
[7] M. W. Knight, H. Sobhani, P. Nordlander, and N. J. Halas, Science **332**, 702 (2011).
[8] N. Lapshina, R. Noskov, and Y. Kivshar, Opt. Lett. **37**, 3921 (2012).
[9] A. Alù and N. Engheta, Phys. Rev. Lett. **104**, 213902 (2010).
[10] C. A. Balanis, *Antenna Theory: Analysis and Design* (John Wiley & Sons: Hoboken, NJ, 2016).
[11] J. Li, A. Salandrino, and N. Engheta, Phys. Rev. B **79**, 195104 (2009).
[12] T. Kosako, Y. Kadoya, and H. F. Hofmann, Nat. Photonics **4**, 312 (2010).
[13] J. Sun, E. Timurdogan, A. Yaacobi, E. S. Hosseini, and M. R. Watts, Nature **493**, 195 (2013).
[14] D. Dregely, K. Lindfors, M. Lippitz, N. Engheta, M. Totzeck, and H. Giessen, Nat. Commun. **5** (2014).
[15] A. Alù and N. Engheta, IEEE Trans. Antennas Propag. **55**, 3027 (2007).
[16] Z. Ruan and S. Fan, Phys. Rev. Lett. **105**, 013901 (2010).
[17] W. Liu, A. E. Miroshnickenko, D. N. Neshev, and Y. S. Kivshar, ACS Nano **6**, pp. 5489 (2012).
[18] S. D. Campbell and R. W. Ziolkowski, IEEE J. Sel. Topics Quantum Electron. **19**, 4700209 (2013).
[19] I. M. Hancu, A. G. Curto, M. Castro-Lopez, M. Kuttge, and N. F. van Hulst, Nano Lett. **14**, 166 (2013).
[20] W. Liu, J. Zhang, B. Lei, H. Ma, W. Xie, and H. Hu, Opt. Express **22**, 16178 (2014).
[21] I. Liberal, I. Ederra, R. Gonzalo, and R. W. Ziolkowski, Phys. Rev. Appl. **1**, 044002 (2014).
[22] A. E. Krasnok, C. R. Simovski, P. A. Belov, and Y. S. Kivshar, Nanoscale **6**, 7354 (2014).
[23] R. R. Naraghi, S. Sukhov, and A. Dogariu, Opt. Lett. **40**, 585 (2015).
[24] R. W. Ziolkowski, P. Jin, and C.-C. Lin, Proc. IEEE **99**, 1720 (2011).
[25] R. W. Ziolkowski, Phys. Rev. X **7**, 031017 (2017).
[26] "See Supplemental Online Material at http://link.aps.org/supplemental/10.xxxx/physrevlett.yyy.zzzzzz," for details of the canonical problem solution, figures of merit, two-dimensional directivity-aperture size relationship, optimization procedure, design and numerical issues, and additional 5-layer results, which includes Refs. [31–37].
[27] C. A. Balanis, *Advanced Engineering Electromagnetics* (John Wiley & Sons: Hoboken, NJ, 1999).
[28] L. Schwartz, *Mathematics for the Physical Sciences* (Addison-Wesley: Reading, MA, 1966).
[29] N. Engheta and R. W. Ziolkowski, *Metamaterials: Physics and Engineering Explorations* (John Wiley & Sons: Hoboken, NJ, 2006).
[30] I. Liberal, I. Ederra, R. Gonzalo, and R. W. Ziolkowski, J. Opt. **17**, 072001 (2015).
[31] R. O. Thorsen, *Electromagnetic Analysis of Nanoparticles in Time and Frequency Domain*, MS diploma thesis, Technical University of Denmark (DTU), Lyngby, Denmark (2016).
[32] S. Arslanagić, R. W. Ziolkowski, and O. Breinbjerg, Radio Sci. **42**, RS6S15 (2007).
[33] E. J. J. Bowman, T. B. A. Senior, and P. L. E. Uslenghi, *Electromagnetic and Acoustic Scattering by Simple Shapes* (North-Holland Publishing Company: Amsterdam, 1969).
[34] W. C. Chew, *Waves and Fields in Inhomogeneous Media* (Van Nostrand Reinhold: New York, 1990).
[35] M. Abramowitz and I. A. Stegun, *Handbook of Mathematical Functions* (Dover Publications: New York, 1965).
[36] R. F. Harrington, IEEE Trans. Antennas Propag. **6**, 219 (1958).
[37] C. Wang, E. Li, and D. F. Sievenpiper, IEEE Trans. Antennas Propag. **65**, 5052 (2017).